CHEMISTRY OF MATERIALS

Article

pubs.acs.org/cm

Atomic Layer Deposition of Titanium Oxide on Single-Layer Graphene: An Atomic-Scale Study toward Understanding Nucleation and Growth

Yucheng Zhang,*[,†] Carlos Guerra-Nuñez,[‡] Ivo Utke,[‡] Johann Michler,[‡] Piyush Agrawal,[†] Marta D. Rossell,[†] and Rolf Erni[†]

[†]Electron Microscopy Center, Empa, Swiss Federal Laboratories for Materials Science and Technology, Überlandstrasse 129, CH-8600 Dübendorf, Switzerland

[‡]Laboratory of Mechanics of Materials and Nanostructure, Empa, Swiss Federal Laboratories for Materials Science and Technology, Feuerwerkstrasse 39, CH-3602 Thun, Switzerland

Supporting Information

ABSTRACT: Controlled synthesis of a hybrid nanomaterial based on titanium oxide and single-layer graphene (SLG) using atomic layer deposition (ALD) is reported here. The morphology and crystallinity of the oxide layer on SLG can be tuned mainly with the deposition temperature, achieving either a uniform amorphous layer at 60 °C or ∼2 nm individual nanocrystals on the SLG at 200 °C after only 20 ALD cycles. A continuous and uniform amorphous layer formed on the SLG after 180 cycles at 60 °C can be converted to a polycrystalline layer containing domains of anatase TiO_2 after a postdeposition annealing at 400 °C under vacuum. Using aberration-corrected transmission electron microscopy (AC-TEM), characterization of the structure and chemistry was performed on an atomic scale and provided insight into understanding the nucleation and growth. AC-TEM imaging and electron energy loss spectroscopy revealed that rocksalt TiO nanocrystals were occasionally formed at the early stage of nucleation after only 20 ALD cycles. Understanding and controlling nucleation and growth of the hybrid nanomaterial are crucial to achieving novel properties and enhanced performance for a wide range of applications that exploit the synergetic functionalities of the ensemble.

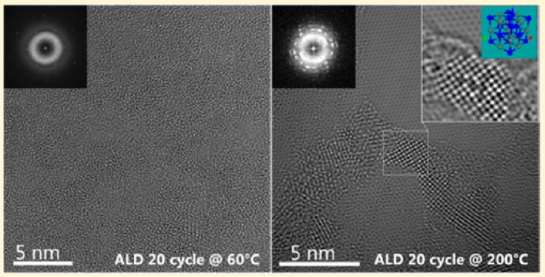

1. INTRODUCTION

Functionalization of carbon-based nanomaterials with metal oxides exploits synergetic combination of the two complementary material systems, promoting enhanced performance and novel functionalities that could be beneficial for a wide range of applications. In particular, applications such as solar cells, batteries, nanoelectronics, and biosensors can benefit from the combination of the superior mechanical strength, high electrical conductivity, and large specific surface of single-layer graphenes (SLGs)[1−3] with the large energy bandgap, superior photocatalytic property, and biocompatibility of TiO_2.[4−6] Consequently, there has been increasing research interest in the hybrid nanomaterial, and a great deal of research effort has been spent to understand and control its synthesis.[7]

Among all the techniques for synthesizing the hybrid nanomaterial, atomic layer deposition (ALD) is the most suitable. The deposition technique relies on self-limiting surface reactions of two precursors that are introduced into the reaction chamber in a sequential manner. Therefore, it allows deposition of conformal layers of metal oxides with a monolayer precision.[8,9] It is particularly suitable for nanostructures with a large aspect ratio such as carbon nanotubes (CNTs) and SLGs. A great deal of research effort has been spent to elaborate the carbon nanomaterials with ALD of metal oxides.[10−13] For instance, Robinson et al. studied the impact of ALD of TiO_2 on the electronic properties of epitaxial graphenes for the development of graphene-based transistors and found that a continuous and amorphous TiO_2 coverage appeared to improve graphene mobility.[14] Ban et al. deposited an amorphous and conformal TiO_2 layer on graphene sheets, which demonstrated its potential as an electrode material in a Li-ion battery.[15] Merchant et al. fabricated nanopores in free-standing graphene sheets for DNA translocations and reported reductions in the ionic current noise level of orders of magnitude when the graphene was covered with 15 nm TiO_2.[16] On the other side, Wang et al. achieved a high efficiency in perovskite solar cells that contained nanocomposites made of crystalline TiO_2 nanoparticles and graphenes.[17] These studies indicate that the ideal morphology and nanostructures vary for different applications, necessitating control over the synthesis of the hybrid material. Here we have employed atomic-scale transmission electron microscopy (TEM) for a detailed study of titanium oxide deposited on SLG with ALD, aiming to gain

Received: December 4, 2016
Revised: February 25, 2017
Published: February 27, 2017

DOI: 10.1021/acs.chemmater.6b05143
Chem. Mater. 2017, 29, 2232−2238

insight into the nucleation mechanism and consequently control over the crystallinity and morphology of the ensemble.

2. EXPERIMENTS

Free-standing SLGs sitting on a TEM Cu grid with a carbon lacey network as support were acquired from TedPella. The samples were transferred directly into a home-built, hot-wall ALD reactor chamber for deposition. Prior to each deposition, the samples were annealed at 200 °C in the chamber for several hours to minimize surface contamination and absorbents. Titanium isopropoxide $Ti[OCH(CH_3)_2]_4$ (TTIP) kept at 90 °C and H_2O at 40 °C were used as precursors with Ar as a carrier gas. The gas delivery lines to the ALD reactor were heated to 100 °C. Every ALD cycle consisted of a 1 s pulse with a 5 s exposure time for each precursor, followed by a 90 s purge for TTIP and a 120 s purge for H_2O using 50 sccm of Ar during pulsing and purging. Twenty cycles of titanium oxide were deposited at 60 and 200 °C. As a comparison, 180 cycles were deposited at 60 °C on another sample, followed by postdeposition *in situ* annealing in the TEM instrument at 400 °C.

The nanostructure was characterized with a JEOL 2200FS TEM instrument operated at 200 kV for diffraction contrast imaging and selected area electron diffraction (SAED). With the same microscope, *in situ* annealing experiments were performed with a Gatan furnace-based heating holder. Atomic-scale TEM imaging was conducted using a JEOL ARM200F microscope equipped with two hexapole type spherical aberration correctors and a cold field-emission gun operated at 80 kV. To further enhance image resolution and contrast, exit-wave reconstruction (EWR) was performed on selected regions by taking a focal series and employing the Gerchberg−Saxton algorithm in MacTempas.[18] For the focal series, 50 images with a focal interval of 1 nm were taken. Electron energy loss spectroscopy (EELS) was performed in TEM mode using a high-speed Enfinium SE spectrometer with an energy resolution around 0.4 eV.

3. RESULTS AND DISCUSSION

Figure 1 shows the atomic-resolution images showing the morphologies of a pristine SLG and the SLGs deposited with titanium oxide after only 20 cycles at 60 and 200 °C. The atomic resolution was achieved using a third-order spherical aberration-corrected microscope, with a small negative value of approximately −10 μm adopted for the third-order spherical aberration coefficient and a small overfocus to optimize the phase contrast with respect to the fixed small positive fifth-order spherical aberration.[19] Under this condition, the carbon atoms in the SLG appear bright with an enhanced contrast, as shown in panel a. Areas of the pristine SLG with the size of a few hundred square nanometers can be routinely observed, decorated with holes, few-layer graphenes, and carbonaceous contaminants that probably stemmed from the film transfer. *In situ* annealing up to 300 °C was found to have a limited effect in removing the contaminants and extending the clean pristine area. The ALD temperature, however, has a dramatic effect on the morphology of the titanium oxide even at the very early stage of the nucleation, i.e., after only 20 cycles, as shown in panels b and c. At 60 °C, the SLG surface appears to be entirely covered with an amorphous layer of titanium oxide. The SLG lattice is not visible in the image, although the fast Fourier transform (FFT) still shows the reflections. In contrast, crystalline nuclei with a size of ∼2 nm were observed at 200 °C. The nuclei are mainly located in the few-layer graphene and contamination region, with the clean pristine region largely free of nucleation, because of the inert nature of SLG. Similar observations were reported for the nucleation of ALD titanium oxide on the surface of CNTs.[20] It is believed that at the low ALD temperature physisorption of precursor molecules is favored on the SLG areas inert to chemisorption; increasing the ALD temperatures desorbs the physisorb water and TTIP molecules effectively, and nucleation is observed on only

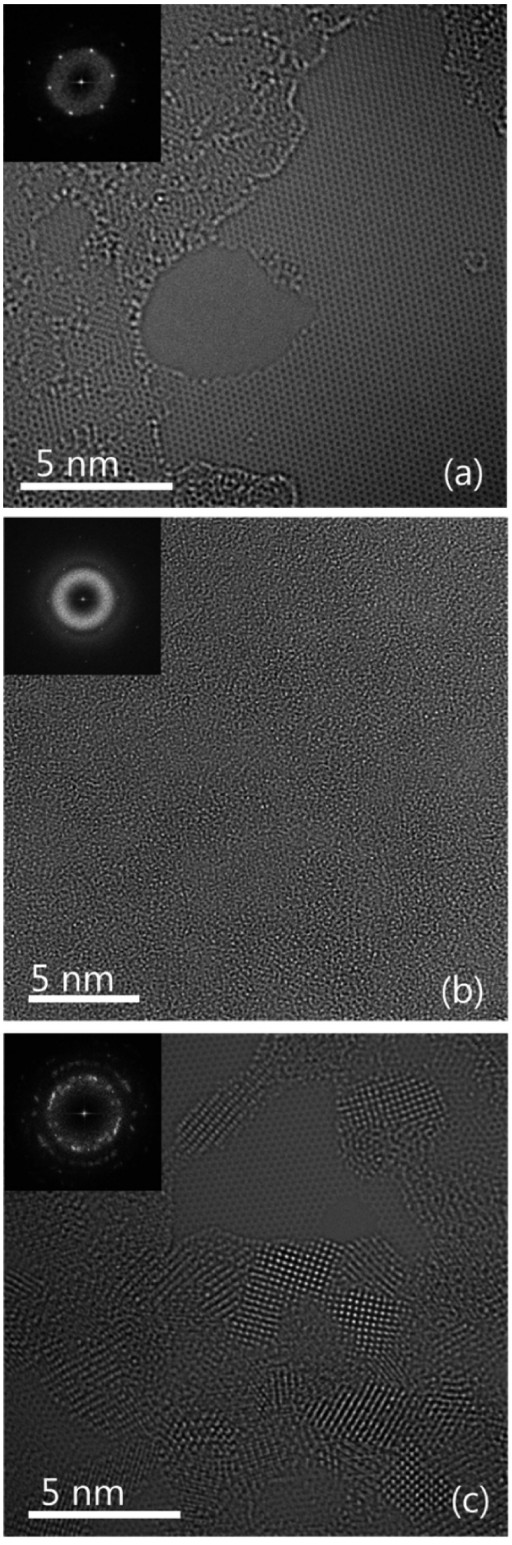

Figure 1. Atomic-resolution TEM images showing the morphology of (a) a pristine single-layer graphene (SLG), (b) a SLG deposited with 20 cycles of titanium oxide at 60 °C, and (c) a SLG deposited with 20 cycles of titanium oxide at 200 °C. The insets show the corresponding Fourier transforms.

DOI: 10.1021/acs.chemmater.6b05143
Chem. Mater. 2017, 29, 2232−2238

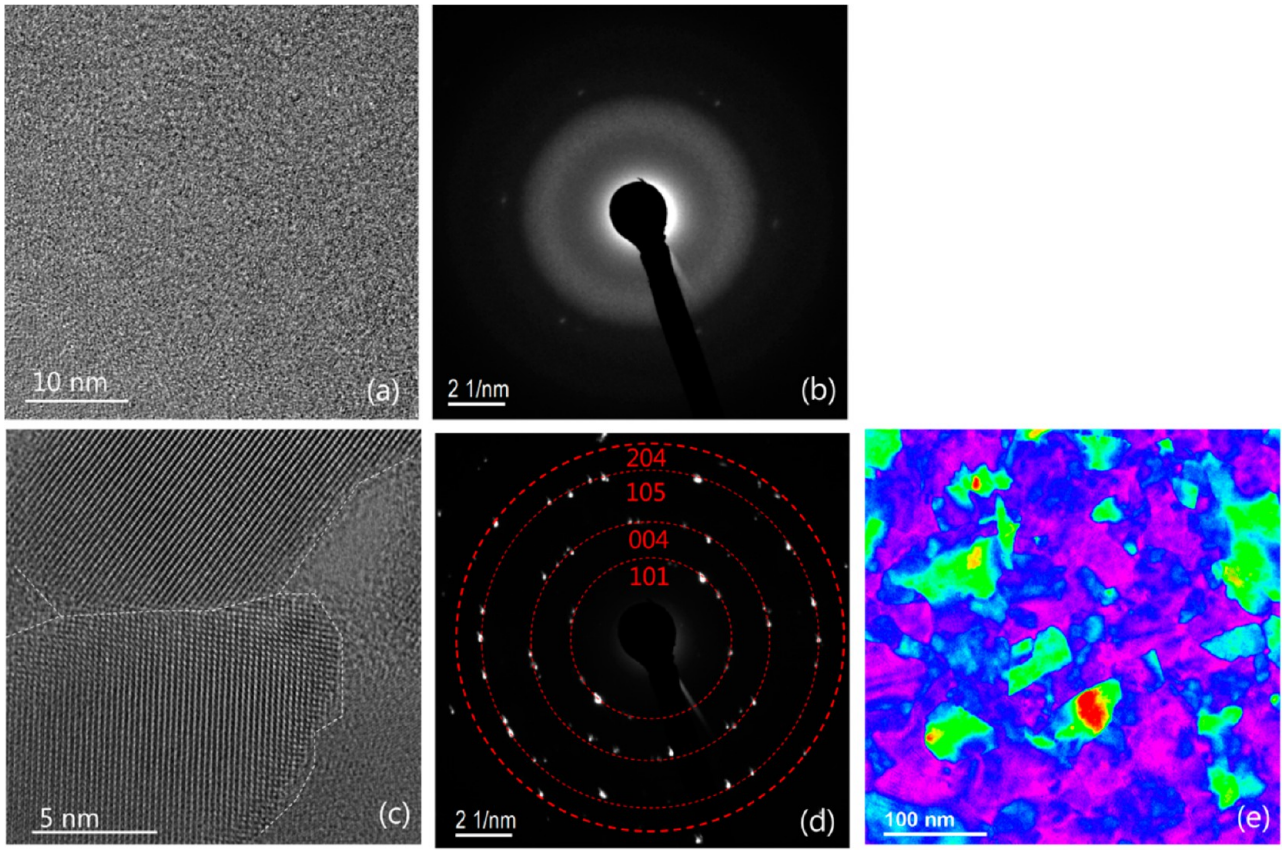

Figure 2. (a) High-resolution TEM image showing the morphology of a SLG deposited with 180 cycles of TiO_2 at 60 °C and (b) the corresponding SAED pattern. (c) Formation of the crystalline grains in the sample after *in situ* annealing at 400 °C and (d) the corresponding SAED pattern. (e) Color-coded BF image showing the distribution of the grains after annealing.

surface defect sites or sites with reactive groups allowing the formation of a thermodynamically stronger chemical bond.

The morphology of the titanium oxide layer can be further modified with a postdeposition annealing at a high temperature under vacuum, to convert the uniform amorphous layer to a conformal crystalline film. Using this method, an ∼10 nm thin monocrystalline anatase TiO_2−CNT core−shell nanostructure was achieved, in which a conformal anatase layer composed of large domains free of defects was formed to surround the CNTs.[21] The same procedure was applied here to the titanium oxide on SLG. A uniform coverage of amorphous titanium oxide on the SLG surface was first obtained after 180 ALD cycles at 60 °C, as shown in panels a and b of Figure 2. The film thickness was ∼20 nm, measured using the log ratio method in EELS.[22] Because of the free-standing geometry of the graphene layer on the Cu grid, the film is deposited on both sides, so that the thickness of each layer is ∼10 nm. This renders a growth per cycle (GPC) of ∼0.05 nm/C at 60 °C. The sample was annealed *in situ* at 400 °C under vacuum in the TEM instrument, i.e., ∼ 2×10^{-5} Torr. Large crystalline domains were instantaneously formed as soon as the temperature reached 400 °C. The boundary between two such domains is delineated in Figure 2c. The indexed SAED pattern in Figure 2d indicates the mere presence of the anatase phase. The size of the domains extends up to a few hundred nanometers, as shown in the color-coded bright field (BF) image in Figure 2e. Within each domain, no defects such as dislocations or stacking faults were observed. Therefore, a continuous layer consisting of large anatase domains on SLG can be formed via this postdeposition annealing method.

Upon deposition at 200 °C, crystalline titanium oxide nuclei of ∼2 nm were routinely observed at the very early stage, i.e., after only 20 ALD cycles, as shown in Figure 1c. It is particularly interesting to further study the nuclei because this knowledge can provide clues about the nucleation mechanism. Figure 3 represents an atomic-scale investigation into the atomic structure of the nuclei. Figure 3a is an overview image in which many such nuclei are readily visible. Among the nuclei oriented in a major zone axis, a crystal lattice with a square symmetry is often observed, with one example shown in Figure 3b. Exit-wave reconstructed (EWR) phase images were attained from focal series of the two regions in panel b, the phase image of a titanium oxide nucleus acquired from the red box shown in panel c, and that of the SLG from the blue box shown in panel d. It is clear that the resolution and contrast are enhanced in the phase images, from which the distance between the atomic columns can be accurately measured. The statistics are presented in panel e.

While the lattice spacing for the SLG matches well with the theoretical value, the measured distance between the two nearest atomic columns for the titanium oxide nucleus, 2.10 Å, is >10% higher than the theoretical value for anatase TiO_2, 1.89 Å,[24] despite the fact that a projection of the TiO_2 lattice in the [001] direction should also possess the square symmetry. Instead, a rocksalt TiO lattice[25] would match well with the measurement. In addition, the variation in intensity among the atomic columns indicates vacancies and nonstoichiometry,

DOI: 10.1021/acs.chemmater.6b05143
Chem. Mater. 2017, 29, 2232−2238

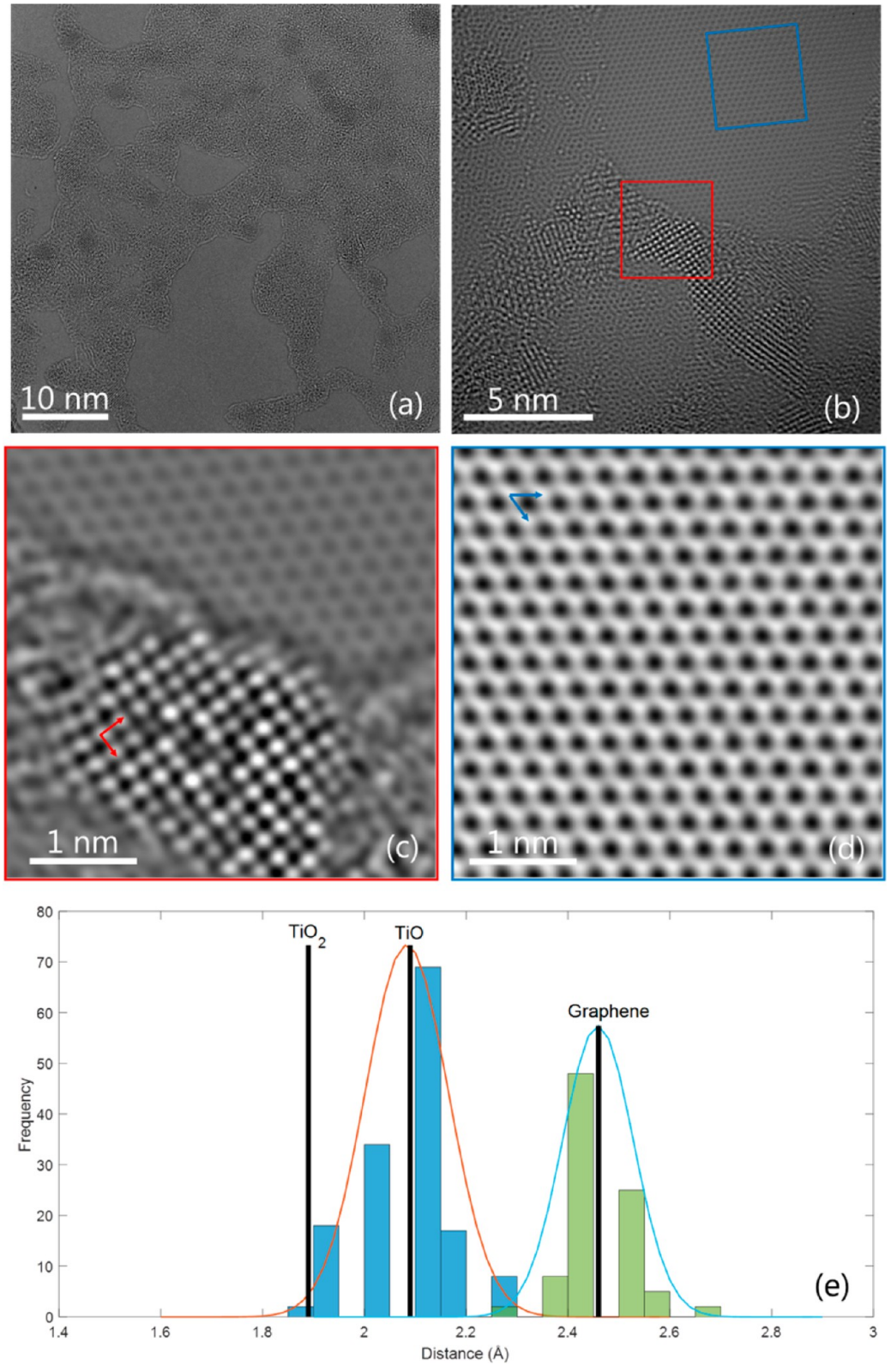

Figure 3. (a) HR-TEM image with a large field of view showing many ∼2 nm titanium oxide nuclei after 20 ALD cycles at 200 °C on SLG. (b) One image from the focal series with the selected regions for exit-wave reconstruction. The phase images of the reconstructed wave showing one nucleus and the graphene lattice are shown in panels c and d, respectively. (e) Measured distances between the atomic columns (denoted by the arrows) compared with the theoretical lattice constants of SLG, anatase TiO_2, and rocksalt TiO.

which are often found in the defect rocksalt structure.[26] For all the observed nuclei with the square symmetry in other regions, the measured lattice constant always corresponds well with that of the rocksalt TiO. However, the observation of the rocksalt lattice is quite sporadic, indicating a small amount of TiO nuclei, presumably <1%, which could not be detected by X-ray

DOI: 10.1021/acs.chemmater.6b05143
Chem. Mater. 2017, 29, 2232−2238

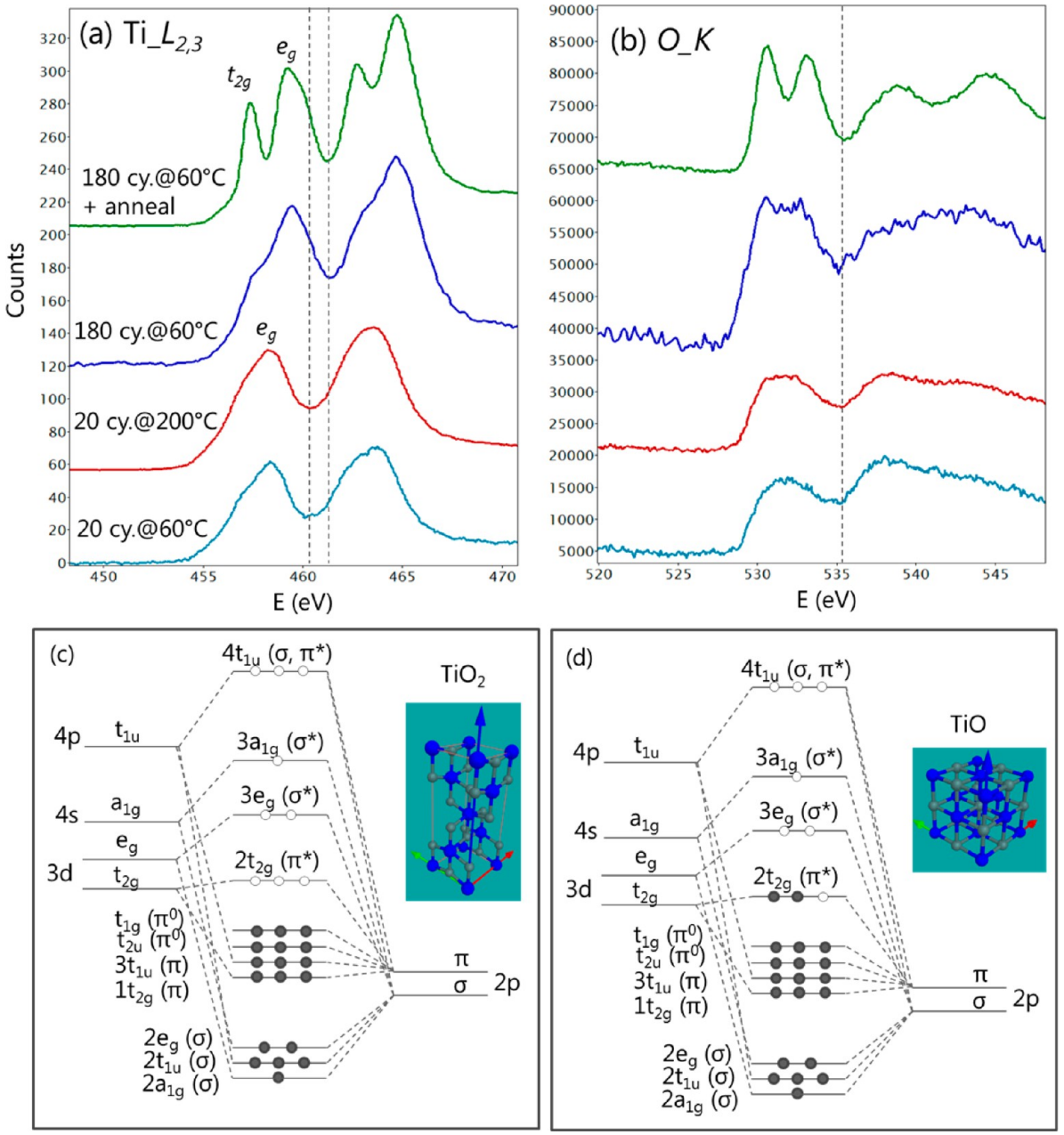

Figure 4. (a and b) EELS spectra showing the Ti_$L_{2,3}$ and O_K edges, acquired from the ALD titania on SLG after 20 cycles at 60 °C, 20 cycles at 200 °C, and 180 cycles at 60 °C and after *in situ* annealing at 400 °C, respectively. The dashed lines in panel a denote the ∼1 eV energy shift due to different oxidation states of Ti. (c and d) Molecular orbitals for anatase TiO_2 and rocksalt TiO (adapted from ref 23), together with their unit cell of the crystal lattice. The main difference is the occupancy of the $2t_{2g}$ (π^*) state, which explains the edge features in the EELS spectra.

photoelectron spectroscopy (XPS). At later stages of growth, TiO nuclei do not seem to persist as the rocksalt lattice was never observed in the film of 180 cycles. This also indicates that for nucleation of <20 cycles, the ratio may be larger than 1% and TiO be an intermediate phase at the initial growth. However, such a hypothesis would need to be clarified with complementary analysis techniques, such as *in situ* TEM.

Electron energy loss spectroscopy (EELS) provided additional evidence that the titanium oxide in a reduced form is present at the early stage of nucleation. EELS spectra from the samples, including 20 cycles at 60 and 200 °C, 180 cycles at 60 °C, and 180 cycles at 60 °C with postdeposition annealing, were obtained. Fine structures near the Ti_$L_{2,3}$ edge and O_K edge were examined and are presented in Figure 4. Two features were identified. First, the Ti_$L_{2,3}$ edge from the annealed sample shows clearly splitting peaks, which is much less prominent in the unannealed sample after 180 cycles and almost completely absent for the samples after 20 cycles. The peak splitting can be explained well by the molecular orbital (MO) theory for oxides.[23] The MOs for all the titanium oxides with different oxidation states are similar, but the occupancy of each orbital depends on the oxidation state and atomic coordination. Sketches of the MOs for anatase TiO_2 and rocksalt TiO are shown in panels c and d of Figure 4, together with their unit cells. In the former, the MOs are occupied up to the t_{1g} level and the $2t_{2g}$ level is empty. In EELS, the electrons in the Ti_$2p$ core levels can therefore be excited to the empty $2t_{2g}$ and $3e_g$ levels, resulting in the observed peak splitting of

DOI: 10.1021/acs.chemmater.6b05143
Chem. Mater. 2017, 29, 2232−2238

the $L_{2,3}$ edges. For the rocksalt TiO, the $2t_{2g}$ level is already filled with electrons and the first available orbital for the excited electrons is the $3e_g$ level, hence, the disappearance of the $2t_{2g}$ peak in the EELS spectra. For any titanium oxide with the Ti valence between Ti^{4+} and Ti^{2+}, the $2t_{2g}$ level would be half-filled and the $2t_{2g}$ peak in the Ti_$L_{2,3}$ edge becomes correspondingly less prominent. For the O_K edge, the same reason applies to the observed splitting peaks. Second, a small energy shift of ∼1 eV in the Ti_$L_{2,3}$ edge was observed upon comparison of the 20-cycle samples with the 180-cycle samples, as denoted by the dotted line. This energy shift, also known as the chemical shift, can be explained by the core−hole effect in EELS. The hole created in the inner shell during the excitation of the electron is screened by the electrons in the outer shell. For the anatase TiO_2, the screening effect is much less due to the unoccupied $2t_{2g}$ level, and consequently, the Ti_$L_{2,3}$ edge is shifted to the higher-energy losses compared to that of metallic Ti. The screening of the core−hole for the TiO is much stronger, because the $2t_{2g}$ level is occupied. In this case, the energy loss is almost similar to that for metallic Ti and, hence, red-shifted with respected to that for the anatase TiO_2. Indeed, the spectra observed here correspond well with those for different Ti_xO_y phases in the study by Stoyanov.[27] Consistent with the observation in the atomic-resolution images, the EELS spectra also indicate the presence of reduced TiO_x, in particular in the form of rocksalt TiO, at the early stage of nucleation after 20 ALD cycles at 200 °C. In addition, EELS simulation of the Ti_L edge was performed using a real space multiple-scattering method. Spectra from anatase TiO_2 under strain were calculated (see Figure S1). The simulation also supports the finding that the observed crystalline nuclei are rocksalt TiO instead of ∼10% strained anatase TiO_2.

Here we would rule out the possibility that the formation of the rocksalt TiO is due to an electron beam effect such as electron-stimulated desorption (ESD)[31,32] of oxygen during the TEM analysis. The acceleration voltage of the incident beam is 80 kV, lower than the threshold value of the knock-on damage for the carbon atoms in the graphene, as well as the oxygen and titanium atoms in the crystalline bulk. For carbon atoms on the edge of a hole or oxygen and titanium atoms weakly bonded on the surface, the knock-on damage is still possible at this energy. On the other hand, the incident energy is also much higher than the usual voltage (∼1 kV) in ESD; therefore, the cross section for desorption of ions from the surface should be much smaler. In addition, if the formation of TiO were caused by the ESD of oxygen, it should form only on the surface. However, the TEM image (as in Figure 3b) clearly shows the same lattice through the thickness. The observation of reduced TiO_x was also reported previously for ALD of titanium oxide on multiwalled CNTs (MWCNTs) using the same precursors.[20] In addition, an *in situ* X-ray photoemission spectroscopy (XPS) study of ALD of TiO_2 on a silicon substrate revealed the presence of Ti^{3+} at the initial stage, i.e., after only two cycles.[28] However, the amount of reduced TiO_x in our sample is believed to be small, probably <1%, beyond the limit of detection of XPS. Only the high spatial resolution offered by the TEM analysis adopted here allows for identification of the species. The formation of the reduced oxides, particularly the rocksalt TiO, and its possible transition to the stoichiometric TiO_2 are not fully understood.

Coating a 5−10 nm conformal layer of TiO_x on CNTs by ALD and using the hybrid as an electron transport layer in inverted organic photovoltaic cells (OPVCs), Jin et al. found that the charge selectivity for the OPVCs was improved.[29] The energy bandgap of the titanium oxide varies with the oxidation state, TiO_2 being a wide bandgap semiconductor, Ti^{3+} oxides having a narrow bandgap, and TiO possessing metallic conductivity. Therefore, engineering of the oxide state provides the option of tuning the light absorption of titanium oxide into the visible range. Indeed, using a doping method, rocksalt TiO nanocrystals have been synthesized and exhibited a very large shift of the light absorption threshold, up to 1.2 eV toward the visible range, compared with that of the anatase TiO_2.[30] However, it appears that the rocksalt TiO and possibly other TiO_x species exist in ALD only at the early stage of nucleation when the deposited layer is ultrathin. As the ALD proceeds and the layer becomes thick, the stoichiometry becomes TiO_2, forming an anatase phase afterward when the sample is annealed at a high temperature. Further investigation is required to understand how the transformation takes place during the growth stage.

4. CONCLUSIONS

Through a detailed TEM characterization of titanium oxide deposited on SLGs, we provide an understanding of ALD nucleation and growth. By tuning the deposition parameters such as the temperature and the number of cycles, one can achieve various morphologies of titanium oxide films on the inert SLG surface: an amorphous layer with uniform coverage was obtained at a low temperature of 60 °C, decoration of ∼2 nm nanocrystals at a high temperature of 200 °C, and a continuous film consisting of laterally extended anatase crystals on the SLG obtained via postdeposition annealing at 400 °C under vacuum. AC-TEM imaging provides direct evidence of the occasional presence of the rocksalt TiO structure at the early stage of nucleation, which is also consistent with the chemical analysis using EELS. This study thus paves the way for atomic-scale engineering of the interface between metal oxides and graphenes using ALD.

■ ASSOCIATED CONTENT

Supporting Information

The Supporting Information is available free of charge on the ACS Publications website at DOI: 10.1021/acs.chemmater.6b05143.

EELS simulation of anatase TiO_2 under 2, 5, and 10% strain and rocksalt TiO using real space multiple scattering, to compare with the experimental data in the main text (PDF)

■ AUTHOR INFORMATION

Corresponding Author

*E-mail: Yucheng.Zhang@empa.ch.

ORCID

Yucheng Zhang: 0000-0003-3733-5851

Notes

The authors declare no competing financial interest.

■ ACKNOWLEDGMENTS

Y.Z. acknowledges the financial support of the EMPA COFUND fellowship scheme funded by the Marie Curie action of the European Commission. I.U. acknowledges SNF funding under Sinergia Project CRSII2_ 147615/1. Y.Z. and R.E. acknowledge funding from the European Research Council

DOI: 10.1021/acs.chemmater.6b05143
Chem. Mater. 2017, 29, 2232−2238

(ERC) under EU's Horizon 2020 program (Grant Agreement 681312). Access to the TEM facilities at IBM Research (Zürich, Switzerland) under the IBM/Empa Master Joint Development Agreement is gratefully acknowledged.

REFERENCES

(1) Ferrari, A. C.; et al. Science and technology roadmap for graphene, related two-dimensional crystals, and hybrid systems. *Nanoscale* **2015**, *7*, 4598−4810.
(2) Geim, A. K.; Novoselov, K. S. The rise of graphene. *Nat. Mater.* **2007**, *6*, 183−191.
(3) Geim, A. K. Graphene: Status and Prospects. *Science* **2009**, *324*, 1530−1534.
(4) Chandiran, A. K.; et al. Sub-Nanometer Conformal TiO2 Blocking Layer for High Efficiency Solid-State Perovskite Absorber Solar Cells. *Adv. Mater.* **2014**, *26*, 4309−4312.
(5) Fujishima, A.; Honda, K. Electrochemical photolysis of water at a semiconductor electrode. *Nature* **1972**, *238*, 37−38.
(6) Gratzel, M. Photoelectrochemical cells. *Nature* **2001**, *414*, 338−344.
(7) Meng, X. B.; Geng, D. S.; Liu, J. A.; Li, R. Y.; Sun, X. L. Controllable synthesis of graphene-based titanium dioxide nanocomposites by atomic layer deposition. *Nanotechnology* **2011**, *22*, 165602.
(8) George, S. M. Atomic Layer Deposition: An Overview. *Chem. Rev.* **2010**, *110*, 111−131.
(9) George, S. M.; Ott, A. W.; Klaus, J. W. Surface chemistry for atomic layer growth. *J. Phys. Chem.* **1996**, *100*, 13121−13131.
(10) Zhang, Y.; et al. Growth and characterization of CNT-TiO2 heterostructures. *Beilstein J. Nanotechnol.* **2014**, *5*, 946−955.
(11) Guerra-Nunez, C.; et al. Morphology and crystallinity control of ultrathin TiO2 layers deposited on carbon nanotubes by temperature-step atomic layer deposition. *Nanoscale* **2015**, *7*, 10622−10633.
(12) Marichy, C.; Bechelany, M.; Pinna, N. Atomic Layer Deposition of Nanostructured Materials for Energy and Environmental Applications. *Adv. Mater.* **2012**, *24*, 1017−1032.
(13) Marichy, C.; Pinna, N. Carbon-nanostructures coated/decorated by atomic layer deposition: Growth and applications. *Coord. Chem. Rev.* **2013**, *257*, 3232−3253.
(14) Robinson, J. A.; et al. Epitaxial Graphene Materials Integration: Effects of Dielectric Overlayers on Structural and Electronic Properties. *ACS Nano* **2010**, *4*, 2667−2672.
(15) Ban, C. M.; et al. Atomic layer deposition of amorphous TiO2 on graphene as an anode for Li-ion batteries. *Nanotechnology* **2013**, *24*, 424002.
(16) Merchant, C. A.; et al. DNA Translocation through Graphene Nanopores. *Nano Lett.* **2010**, *10*, 2915−2921.
(17) Wang, J. T. W.; et al. Low-Temperature Processed Electron Collection Layers of Graphene/TiO2 Nanocomposites in Thin Film Perovskite Solar Cells. *Nano Lett.* **2014**, *14*, 724−730.
(18) Gerchberg, R. W.; Saxton, W. O. Practical Algorithm for Determination of Phase from Image and Diffraction Plane Pictures. *Optik* **1972**, *35*, 237−246.
(19) Lentzen, M. Contrast transfer and resolution limits for sub-angstrom high-resolution transmission electron microscopy. *Microsc. Microanal.* **2008**, *14*, 16−26.
(20) Zhang, Y.; et al. Understanding and Controlling Nucleation and Growth of TiO2 Deposited on Multiwalled Carbon Nanotubes by Atomic Layer Deposition. *J. Phys. Chem. C* **2015**, *119*, 3379−3387.
(21) Zhang, Y.; et al. High Conformity and Large Domain Monocrystalline Anatase on Multiwall Carbon Nanotube Core-Shell Nanostructure: Synthesis, Structure, and Interface. *Chem. Mater.* **2016**, *28*, 3488−3496.
(22) Egerton, R. F. *Electron Energy Loss Spectroscopy in the Electron Microscope*, 3rd ed.; Springer: Dordrecht, The Netherlands, 2000.
(23) Fischer, D. W. Molecular-orbital interpretation of soft X-ray LII,III emission and ebsorption spectra from some titanium and vanadium Compounds. *J. Appl. Phys.* **1970**, *41*, 3561−3569.
(24) Weirich, T. E.; Winterer, M.; Seifried, S.; Hahn, H.; Fuess, H. Rietveld analysis of electron powder diffraction data from nanocrystalline anatase, TiO2. *Ultramicroscopy* **2000**, *81*, 263−270.
(25) Yu, T.-H.; Lin, S.-J.; Chao, P.; Fang, C.-S.; Huang, C.-S. A preliminary study of some new minerals of the platinum-group and another associated new one in platinum-bearing intrusions in a region of China. *Dizhi Xuebao* **1974**, *2*, 202−218.
(26) Wiberg, E.; Wiberg, N. *Inorganic Chemistry*; Academic Press: San Diego, 2001.
(27) Stoyanov, E.; Langenhorst, F.; Steinle-Neumann, G. The effect of valence state and site geometry on Ti L-3,L-2 and OK electron energy-loss spectra of TixOy phases. *Am. Mineral.* **2007**, *92*, 577−586.
(28) Lee, S. Y.; et al. In-situ X-ray Photoemission Spectroscopy Study of Atomic Layer Deposition of TiO2 on Silicon Substrate. *Jpn. J. Appl. Phys.* **2012**, *51*, 3031102.
(29) Jin, S. H.; Jun, G. H.; Hong, S. H.; Jeon, S. Conformal coating of titanium suboxide on carbon nanotube networks by atomic layer deposition for inverted organic photovoltaic cells. *Carbon* **2012**, *50*, 4483−4488.
(30) Simon, P.; et al. N-Doped Titanium Monoxide Nanoparticles with TiO Rock-Salt Structure, Low Energy Band Gap, and Visible Light Activity. *Chem. Mater.* **2010**, *22*, 3704−3711.
(31) Madey, T. E. Electron-Stimulated and Photon-Simulated Desorption - Probes of Structure and Bonding at Surfaces. *Science* **1986**, *234*, 316−322.
(32) Humphreys, C. J.; Bullough, T. J.; Devenish, R. W.; Maher, D. M.; Turner, P. S. Electron-Beam Nano-Etching in Oxides, Fluorides, Metals and Semiconductors. *Scanning Microscopy* **1990**, 185−192.

DOI: 10.1021/acs.chemmater.6b05143
Chem. Mater. 2017, 29, 2232−2238